CellPress
OPEN ACCESS

Trends in
Plant Science

Review

Form follows function – structural interplay between DCL1 and pri-miRNAs

Cecile R. Scholl [1,7], Lars Grosch [2,7], Jana Baradei [3], Panagiotis L. Kastritis [3,4,5], Clara T. Schoeder [2,6], and Sascha Laubinger [1,*]

MicroRNAs (miRNAs) guide post-transcriptional gene silencing in plants and shape developmental outcomes and environmental responses by precisely tuning gene expression. miRNAs originate from primary transcripts (pri-miRNAs) whose structural features – including internal loops, mismatches, and sequence motifs – facilitate interactions with the miRNA processing complex composed of DICER-LIKE 1 (DCL1), HYPONASTIC LEAVES 1 (HYL1), and SERRATE (SE). *In vitro* structural analyses of DCL1, HYL1, and SE proteins have elucidated their interactions with each other and with pri-miRNAs at unprecedented resolution. These findings highlight plant-specific processing features that are distinct from those of animals and suggest new avenues for manipulating miRNA pathways. We review recent progress in understanding the structural determinants of pri-miRNA processing, knowledge that may also be valuable for future applications in crop species through targeted genome editing.

Highlights

Plant pri-miRNAs exhibit remarkable structural diversity and are processed via five distinct pathways, each guided by specific structural rulers and motifs that influence cleavage sites.

RNA secondary structure (RSS) is the key determinant of pri-miRNA processing efficiency and precision. Recent findings highlight that accurate RSS characterization primarily requires experimental validation rather than relying solely on computational predictions.

Cryo-electron microscopy (cryo-EM) has revealed the architecture of DCL1 and proposes precise cleavage events. Mutations that alter enzymatic efficiency indicate regulatory mechanisms that are intrinsic to DCL1 structure and function.

Unresolved flexible regions and conflicting biochemical data emphasize the need for integrative structural and functional analyses to fully understand pri-miRNA processing.

From pri-miRNA to function: the intricate world of plant miRNA processing

In plants, microRNAs (miRNAs) 20–22 nt in length play essential roles in controlling plant growth and development [1–4]. Mature miRNAs function by associating with the ARGONAUTE 1 (AGO1) protein (or one of its paralogs) within the miRNA-induced silencing complex (miRISC) where they guide the miRISC to target specific mRNAs for post-transcriptional regulation (Figure 1, Key figure) [1–9].

The process of mature miRNA biogenesis initiates in the nucleus with the transcription of MIRNA genes (*MIR*s) by RNA polymerase II, resulting in primary miRNA transcripts (**pri-miRNAs**; see Glossary) [1,2,5]. Unlike animal pri-miRNAs, plant pri-miRNAs are highly variable in length and architecture and exhibit an imperfect stem–loop structure [10–12]. Processing of these pri-miRNAs involves two sequential cleavage steps to release the miRNA/miRNA* duplex (Figure 1) that are primarily catalyzed by the key enzyme **DICER-LIKE 1 (DCL1)** [10,11]. DCL1 works in concert with other proteins, such as the zinc-finger protein SERRATE (SE) and double-stranded (ds) RNA-binding protein (DRB) HYPONASTIC LEAVES 1 (HYL1), to recognize and process the pri-miRNA into precursor miRNA (pre-miRNA) (Figure 1) [10,11,13]. Following the second cleavage by DCL1, the miRNA/miRNA* duplex, characterized by 2 nt overhangs, is methylated by HUA ENHANCER 1 (HEN1) to prevent degradation, ensuring stability for subsequent steps (Figure 1) [14,15].

Unlike in animals, where miRNA biogenesis involves two distinct enzymes (DROSHA and DICER [16–18], both processing steps of miRNAs in plants are catalyzed by DCL1 [1,2,5]. This plant-specific mechanism increases the complexity of regulation, amplified by the large structural heterogeneity of pri-miRNAs in plants [17,18]. Recent advances in structural biology have provided deeper insights into pri-miRNA architecture and DCL1 protein function [19–22]. These findings

[1]Institute of Biology, Department of Genetics, Martin Luther University Halle-Wittenberg, Halle (Saale), Germany
[2]Institute for Drug Discovery, Medical Faculty, Leipzig University, Leipzig, Germany
[3]Institute of Biochemistry and Biotechnology, Department of Integrative Structural Biochemistry, Martin Luther University Halle-Wittenberg, Halle (Saale), Germany
[4]Biozentrum and Center for Innovation Competence (ZIK) HALOmem, Martin Luther University Halle-Wittenberg, Halle (Saale), Germany
[5]Institute of Chemical Biology, National Hellenic Research Foundation, Athens, Greece
[6]Center for Scalable Data Analytics and Artificial Intelligence (ScaDS.AI), Dresden/Leipzig, Germany
[7]Equal contributions

CellPress
OPEN ACCESS

Key figure

MicroRNA (miRNA) biogenesis: from primary miRNA (pri-miRNA) structure and processing to gene silencing

*Correspondence:
sascha.laubinger@genetik.uni-halle.de
(S. Laubinger).

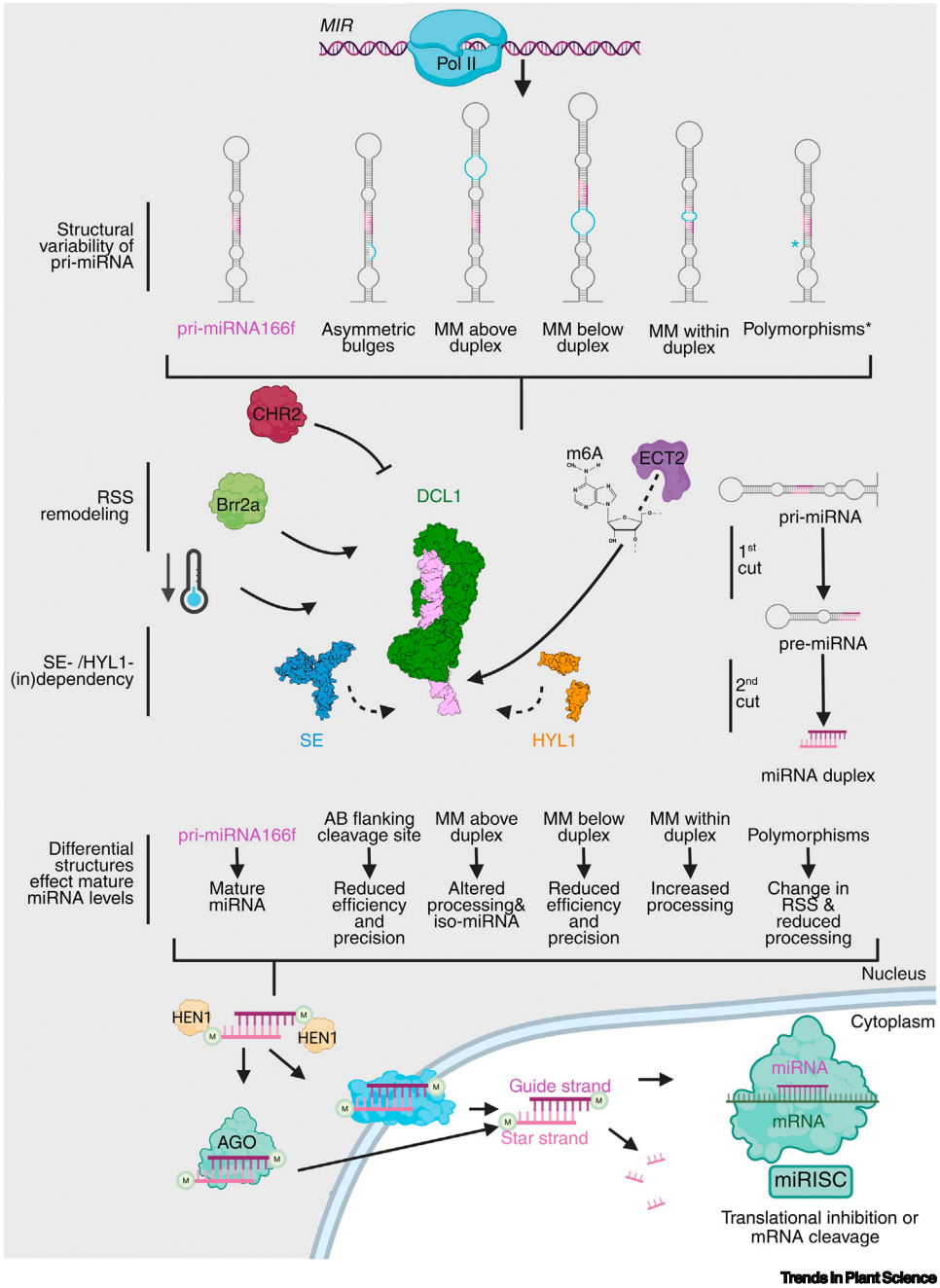

Figure 1. miRNA biogenesis initiates with the transcription of *MIR* genes by RNA polymerase II (Pol II), generating pri-miRNAs transcripts, exemplified here by pri-miRNA166f. Several structural elements, including internal bulges, mismatches (MMs) at different positions, and intra- and interspecies sequence variations (polymorphisms), contribute to the structural diversity of

(Figure legend continued at the bottom of the next page.)

not only highlight unique plant-specific mechanisms in miRNA biogenesis but also raise new questions about how structural diversity influences miRNA processing in plants.

Processing pathways and structural determinants of pri-miRNAs

Unlike in animals, where the DROSHA enzyme initiates pri-miRNA processing [16,17], plants employ five distinct pri-miRNA processing mechanisms to produce mature miRNAs (Figure 2A) [23–28]. The first two pathways are named after their processing direction. (i) In base-to-loop (BTL) processing, the first cleavage occurs in the lower stem of the pri-miRNA precursor, and the second cut takes place ~21 nt upstream in the upper stem [2,27]. (ii) Conversely, loop-to-base (LTB) processing proceeds in the opposite direction, beginning with a cut above the miRNA/miRNA* duplex, followed by a second cut ~21 nt lower in the stem [2,27]. The other two mechanisms – (iii) sequential BTL (SBTL) and (iv) sequential LTB (SLTB) – involve multiple cuts along their elongated structure, following the same directional pattern [13,27]. The fifth pathway, (v) bidirectional processing, can initiate from either the stem or the loop, adding further complexity [13,28].

Recent research combining degradome sequencing and the expression of semi-active DCL1 variants has mapped the exact processing route for almost half of all arabidopsis (*Arabidopsis thaliana*) pri-miRNAs [20]. Findings show that 36% are processed starting at the base, 35% at the loop, and 29% are processed bidirectionally [20]. Bidirectional processing can lead to non-productive outcomes or generate distinct miRNAs targeting different mRNAs [20,28]. The same study systematically revealed that miRNAs are processed at multiple sites to release alternative miRNAs (also known as isomiRs) [20]. A comprehensive databank survey suggests that >20 000 isomiRs are present in arabidopsis [29]. Some isomiRs could represent processing errors, non-functional byproducts, or simply background noise. This widespread alternative processing of pri-miRNAs complicates the identification of structural or sequence motifs that are important for accurate processing.

Given that pri-miRNAs undergo diverse processing pathways, they must exhibit a broader range of specific primary and secondary structures to define their cleavage sites, in contrast to the comparatively simpler metazoan pri-miRNAs [30]. An internal loop positioned 15–17 nt away from the first cleavage site is essential for all types of processing [20,24,26] (Figure 2A). This structure is conserved across multiple DCL1-dependent pri-miRNA and plant species [20,31]. However, this 15–17 nt ruler is not the sole determinant [19,20]. *In vivo* RNA secondary structure (RSS) information revealed an additional smaller internal loop positioned 9–11 nt away from the miRNA/miRNA* duplex that fits the **cryo-electron microscopy (cryo-EM)** density map of DCL1, resolved in a complex with the pri-miRNA166f at 4.6 Å resolution [19,20]. However, the 9–11 nt ruler is more common in LTB processing, whereas the 15–17 nt ruler is more crucial for BTL

Glossary

DICER-LIKE 1 (DCL1): the key enzyme in miRNA biogenesis. Its RNase III domains cleave pri-miRNAs, generating miRNA duplexes with characteristic 2 nt 3′ overhangs.
Dimethyl sulfate mutational profiling and sequencing (DMS-MaPseq): a chemical-based method used to probe RNA secondary structures *in vivo* by treating RNA with DMS, which chemically modifies unpaired adenine and cytosine residues. Modified nucleotides are detected as mutations after reverse transcription and sequencing, enabling high-resolution analysis of RNA secondary structures. Another chemical-based approach, SHAPE-MaP (selective 2′-hydroxyl acylation analyzed by primer extension and mutational profiling), modifies the 2′-OH groups of structurally flexible (unpaired) nucleotides.
Pri-miRNAs: long RNAs from which miRNA duplexes are released. They form hairpin structures and feature characteristic loops and bulges which are recognized by the miRNA processing complex.
Single-particle cryo-electron microscopy (cryo-EM): a structural biology technique for purified imaging biological molecules that are rapidly frozen at cryogenic temperatures to preserve their native hydrated state. To obtain high-resolution spatial information, thousands of high-magnification 2D electron microscopy images are computationally segmented to retrieve up to millions of images. These extracted images are ultimately averaged and combined to reconstruct detailed 3D Coulomb potential maps which are used to model the biomolecular structures at (near-)atomic resolution.

pri-miRNAs and significantly influence their processing efficiency. Furthermore, the position and identity of mismatches strongly affect DCL1-mediated cleavage. The core microprocessor complex comprising DCL1 (green), HYL1 (yellow), and SE (blue) sequentially processes pri-miRNAs into pre-miRNAs and ultimately into mature miRNA duplexes. The illustration is based on the structures of DCL1 (PDB: 7ELD), SE (PDB: 3AX1 [64]), and HYL1 (PDB: 3ADG [62] and PDB: 3ADJ [62]) using the surface representation of ChimeraX. After DCL1-mediated cleavage, miRNA duplexes are released. Although most pri-miRNA processing depends on SE and HYL1, some pri-miRNAs or environmental factors such as reduced temperature can partially bypass this requirement. The miRNA duplex is methylated by HEN1 to prevent degradation and subsequently loaded onto ARGONAUTE (AGO) proteins to form the miRNA-induced silencing complex (miRISC). Following strand separation, mature miRNAs guide the miRISC to complementary target mRNAs, resulting in translational inhibition or cleavage of target mRNAs and thereby repression of gene expression. The asterisk (*) indicates that polymorphisms are found in this structure. Abbreviations: AB, asymmetric bulge; m6A, N^{6}-methyladenosine; RSS, RNA secondary structure.

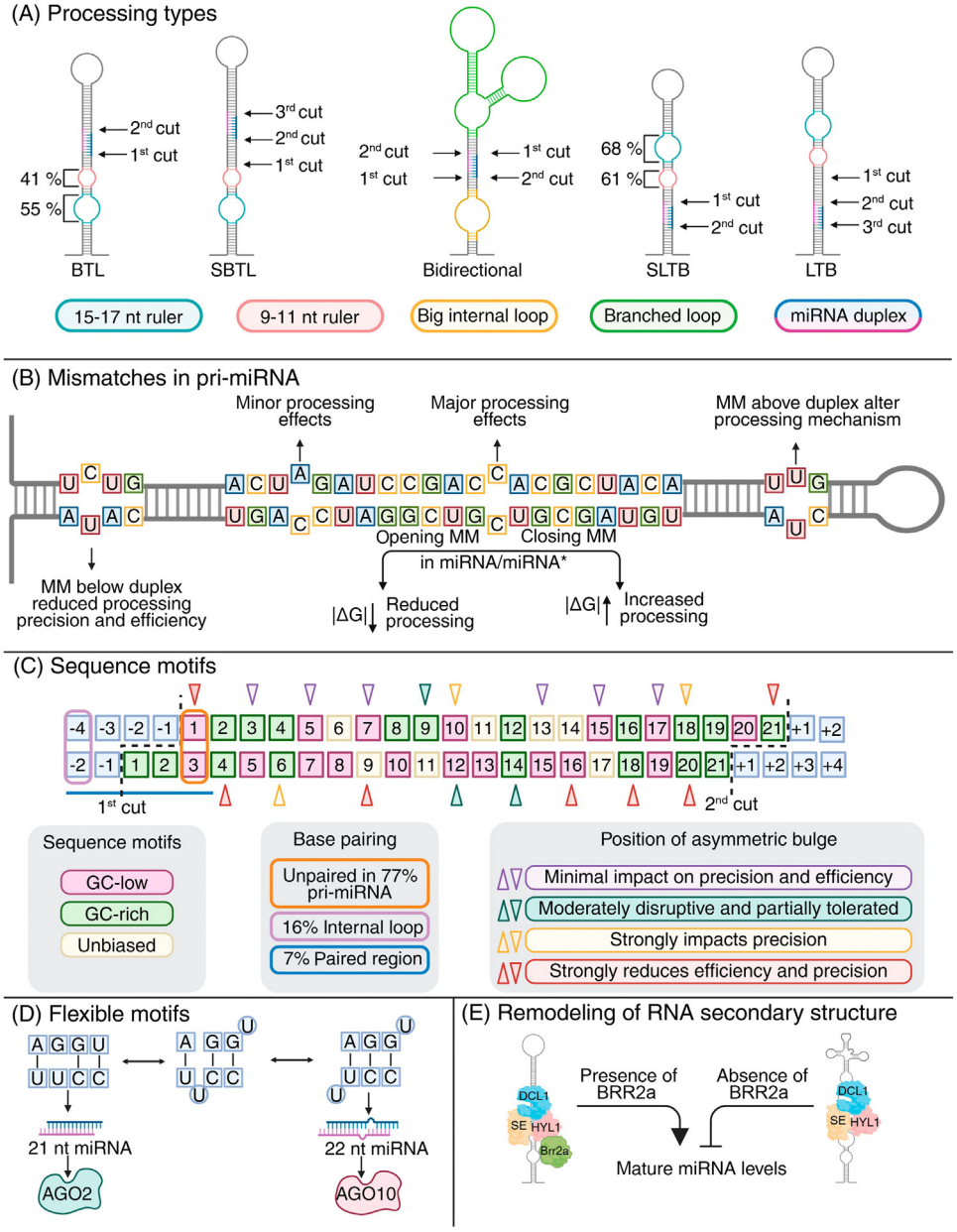

Figure 2. Structural determinants in pri-miRNA processing. (A) Five different pri-miRNA processing pathways have been described in plants: base-to-loop (BTL), sequential base-to-loop (SBTL), bidirectional, loop-to-base (LTB), and sequential loop-to-base (SLTB). Different colors are indicative of key structural determinants for the respective types of processing. In BTL processing, the first initial cut is determined by a 15–17 nt (orange) and 9–11 nt (blue) ruler below the miRNA/miRNA* duplex (bicolor). To release the mature miRNA/miRNA* duplex, DCL1 mediates a second cut 21 nt away from the first. In the LTB processing mechanism, the 15–17 nt and 9–11 nt rulers are located in the upper stem to mark the first cleavage site. The presence of the 9–11 nt and 15–17 nt ranges in the processing types is depicted in percentages. In SBTL and SLTB, mature miRNA generation requires multiple cuts. Bidirectionally processed pri-miRNA can be processed by either the BTL or LTB pathways. Structural motifs marking this type of processing are a big internal loop (yellow) or a terminal branched loop (green) [20]. (B) Effect of mismatch (MM) identity and position on accurate pri-miRNA processing. (C) miRNA/miRNA* duplex depicts the enrichment of GC-rich motifs at different positions of pri-

(Figure legend continued at the bottom of the next page.)

processing (Figure 2A) [20]. This raises the question of how DCL1 preferentially recognizes distinct structural rulers across different processing pathways and why these structures are not uniformly present. Terminal-branched loops have long been described as the key motif in bidirectional processing [28]. Yan *et al.* further showed that bidirectionally processed pri-miRNA contain a large internal loop before the first cleavage site, underscoring the complex relationship between structural elements and processing direction (Figure 2A) [20].

Mismatches in the pri-miRNA stem introduce another layer in pri-miRNA processing. The position of paired and unpaired regions can alter DCL1 cleavage efficiency, leading to variations in miRNA abundance and miRNA isoforms [20,32,33]. Rojas *et al.* identified a high occurrence of paired regions at positions 1, 3, and 23, near to both cleavage sites [32]. Contradictory to these results, *in vivo* RSS determined by **dimethyl sulfate mutational profiling and sequencing (DMS-MaPseq)** revealed that 77% of pri-miRNAs contain an unpaired region at the first cleavage site [20], aligning with previous findings (Figure 2C) [33]. These conflicting findings remain unresolved; however, the RSS derived from *in vivo* approaches, such as DMS-MaPseq, likely better reflects the pri-miRNA structure under physiological conditions. The identity of the mismatches themselves also plays a crucial role. Although C–C mismatches near cleavage sites greatly impair processing, A–C, U–U, and C–U mismatches have a milder impact [32]. This suggests that C–C mismatches introduce some type of hindrance that affects DCL1 binding, compared to other mismatches (Figure 2B) [32]. In addition to mismatch identity, mismatch position within the pri-miRNA can also shift and impair its processing. An increased number of mismatch events decreases miRNA duplex stability, leading to reduced mature miRNA levels [21]. Conversely, decreasing the number of mismatches increases processing efficiency through higher interaction energy and stability (| G|, the absolute value of the change in Gibbs free energy) (Figure 2B). Interestingly, mismatches outside the miRNA duplex also have an impact on processing efficiency. In multiple BTL-processed pri-miRNAs, closing mismatches below the miRNA duplex impaired second-cut precision while leaving the first cut unaffected [33]. Conversely, closing mismatches above the miRNA duplex shifted the processing mechanism from BTL to LTB [33]. Evolutionarily younger miRNAs deriving from sequentially processed pri-miRNAs showed a lower interaction energy, prompting the authors to conclude that mutations leading to mismatches in young miRNA might result in lower DCL1 affinity [21]. Studying younger pri-miRNA structures in different plant lineages and their affinity for DCL1 could be a compelling approach to understanding the evolutionary dynamics of miRNA biogenesis.

Pri-miRNA processing in plants is guided not only by secondary structure but also by sequence motifs. Inside the miRNA/miRNA* duplex, the miRNA processing complex prefers GC-rich motifs at positions 8–9 and 18–19 (Figure 2C) [34]. Further, a GC content of ~52% increased miRNA processing efficiency [34]. Similar trends were observed in siRNAs processed by other DCL homologs [35–37], indicating this primary structure is not exclusive to DCL1-dependent miRNA processing pathways.

miRNAs. Triangles above the nucleotides indicate the effect of asymmetric bulges on different positions within the duplex. Orange boxes display unpaired regions, lilac boxes show the occurrence of internal loops near the first cleavage site, and the blue bar shows paired regions in DCL1-dependent pri-miRNAs. (D) The formation of different pri-miRNA sequence motifs alters their secondary structure. The conformational change induces the generation of 22 nt instead of 21 nt miRNAs, resulting in differential AGO loading and target suppression. (E) Before being processed by the miRNA processing complex, the RNA secondary structure (RSS) of pri-miRNAs can be remodeled by proteins such as BRR2A [43]. In the absence of BRR2A, misfolded pri-miRNA is not precisely processed, resulting in reduced mature miRNA levels. In the presence of BRR2A, pri-miRNA unwinds and folds into its correct secondary structure, increasing the precise generation of mature miRNA. Abbreviations: | G|, the absolute value of the change in Gibbs free energy; MM, mismatch.

However, motif flexibility within one pri-miRNA can highly impact processing. For instance, base-pairing flexibility in pri-miRNA168 enables alternative processing pathways, leading to asymmetric bulge formation and the production of distinct miRNA isoforms (Figure 2D) [38]. These isoforms exhibit different affinities for AGO proteins and influence the downstream silencing efficiency (Figure 2D) [38]. The impact of such base-pairing variations also depends on their position. Although asymmetric bulges in the 5′ arm are generally well tolerated, those in the 3′ arm tend to reduce miRNA maturation significantly (Figure 2C) [22]. This suggests that motif flexibility is not simply tolerated but may serve as an adaptive feature to fine-tune processing outcomes (Figure 2C).

Because RSS is crucial for precise pri-miRNA processing, recent studies unsurprisingly revealed several regulatory factors that influence pri-miRNA structures in arabidopsis (Figure 1) [39–41]. One such protein is chromatin remodeling factor 2 (CHR2), a subunit of the SWI2/SNF2 complex, that remodels pri-miRNAs to regulate their processing negatively (Figure 1) [42]. Unlike CHR2, the RNA helicase BRR2A promotes pri-miRNA processing [43]. BRR2A unwinds pri-miRNA to modify its RSS, thereby enhancing the accessibility of the cleavage site to DCL1 and HYL1 (Figure 2E) [43]. The unwinding mechanism of BRR2A has been studied at (near-)atomic detail, mostly in human and yeast (>100 structures are deposited in the protein data bank, www.pdb.org, as of June 2025), especially by resolving the corresponding spliceosome states involving BRR2A (>60 cryo-EM structures of >1 MDa as of June 2025). Interestingly, arabidopsis BRR2A shares only ~50–60% identity with deposited structures, and is currently unresolved, raising questions regarding plant-specific unwinding mechanisms.

Apart from protein components, covalent RNA modifications can also affect the RSS of pri-miRNAs. The adenosine-methyltransferase MTA methylates adenosines to generate N^6-methyladenosine (m6A) that increases pri-miRNA accessibility to the miRNA processing complex and promotes miRNA processing [44]. This study suggests that m6A-induced methylations occur within the miRNA duplex and stem-loop [44], whereas a more recent study revealed m6A modifications primarily in the single-stranded regions flanking the stem loop [41]. The authors found that m6A modifications recruit ECT2 to pri-miRNAs to enhance their processing efficiency (Figure 1) [41]. Whether there are other RNA modifications of plant pri-miRNAs, as in metazoans [45,46], and whether they influence pri-miRNAs processing, remains to be elucidated.

Structural complexities of DCL1 and their impact on miRNA biogenesis

In addition to structural information about pri-miRNAs, structural insight into the proteins involved in miRNA biogenesis has advanced the field. In arabidopsis, DCL1 is the key enzyme for the biogenesis of most miRNAs, whereas the other three paralogs (DCL2, DCL3, and DCL4) are involved in generating different types of small RNAs [47–51]. DCL1 contains seven known functional domains – a helicase domain, DUF283 (domain of unknown function), a Piwi/Ago/Zwille (PAZ) domain, two RNase III domains, and two dsRNA-binding domains (dsRBDs) [2,50,52]. An overview of the structural model, its domains, and their interaction with the pri-miRNA166f [19] is shown in Figure 3A. The structural model of DCL1 also enables speculation about the structural mechanisms underlying various gain- or loss-of-function *dcl1* alleles (Box 1).

The helicase domain of DCL1 is highly conserved among DICER proteins [50,51]. DCL1 belongs to the DExH/D helicase family, specifically containing a DECH motif [53,54]. In DCL1, the helicase domain and DUF283 supposedly undergo conformational changes when binding to the dsRNA and bend the pri-miRNA backbone by ~23° [19]. After the first cleavage, the pre-miRNA is presumably transferred to the second cleavage site by the helicase [19]. It is hypothesized that the helicase domain exhibits an autoinhibitory regulation because pri-miRNA processing efficiency

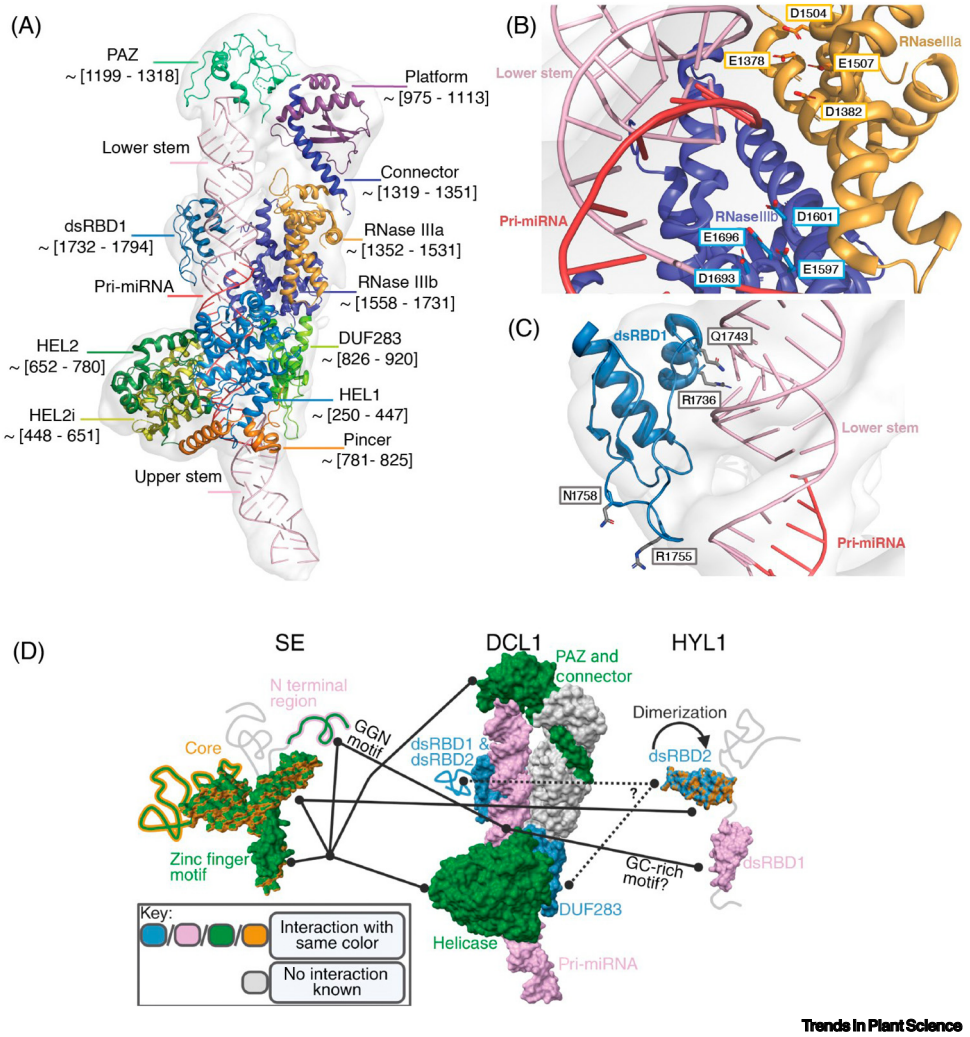

Figure 3. Structure of the DCL1–pri-miRNA complex and its interactions with SE and HYL1. (A) A model of the DCL1/pri-miRNA166f complex (ribbon representation of domains are distinctly colored) fitted into the 4.6 Å cryo-electron microscopy (cryo-EM) density map (transparent surface) used for model reconstruction [19]. (B) Zoom into the cryo-EM structure (A) at the interface between the double-stranded (ds) RNA-binding domain 1 (dsRBD1) and the pri-miRNA; residues are highlighted as gray sticks for carbons, blue for nitrogens, and oxygens are shown in red. (C) Zoom into the cryo-EM structure (panel A) at the interface between the RNase IIIa and RNase IIIb domains and the pri-miRNA166f. Residues are highlighted as sticks and colored in orange for the RNase IIIa domain, and light blue for the RNase IIIb domain. (D) Intermolecular interacting protein domains are depicted with the same color and are connected by a black line. A colored or grey line represents the unstructured regions of SE and HYL1, and all the unstructured regions except the dsRBD2 domain of DCL1 have been omitted for visual conciseness. ChimeraX has been used for the 3D presentation of the following PDB structures in surface representation: DCL1 (PDB: 7ELD [19]), SE (PDB: 3AX1 [64]), and HYL1 (PDB: 3ADG [62] and PDB: 3ADJ [62]). Machida et al. demonstrated interactions of the SE core with HYL1 dsRBD2 domain, as well as with the helicase and PAZ domains of DCL1, by using pull-down assays; however, the proposed interaction between the SE zinc-finger motif and HYL1 remains unvalidated [64]. Iwata et al. reported interactions between DCL1 and the SE zinc finger and its unstructured N-terminal region [61]. Dimerization of HYL1 was demonstrated by coprecipitation and yeast two-hybrid assays [62,67,73]. Finally, multiple domains within DCL1, including DUF283 [55], dsRBD1 [71], and dsRBD2 [57], have been proposed as possible interaction sites for the HYL1 dsRBD2 domain based on coprecipitation, yeast two-hybrid, and biolayer interferometry studies. The N-terminal region of SE was proposed to bind to RNA using surface plasmon resonance (SPR) spectroscopy [61], but later experiment could not confirm this finding [74]. The dsRNA-binding capability of HYL1 dsRBD1 has been validated by electrophoretic mobility shift assay (EMSA) [84] and biolayer interferometry [71]. SE has been found to associate with GGN repeats within RNAs [85] and Narjala et al. found affinity of HYL1 for GC motifs within the miRNA duplex [34].

is increased in a helicase-truncated DCL1 [53]. Because it is homologous to the DCL4 DUF283 domain, the DCL1 DUF283 domain can be classified as a non-canonical dsRBD that exhibits only weak RNA interactions [55]; instead, it mediates the interaction with the dsRBD2 domain of HYL1 [19,55].

The PAZ domain of DCL1 and other DICERs is responsible for binding to the internal loop of pri-miRNA or pre-miRNA overhang [19,50]. It binds to the 5' phosphate of the miRNA strand within a specific pocket and ensures the correct positioning of the dsRNA for cleavage by the RNase III domains [19]. This mechanism is essential for accurate and efficient processing of pri-miRNAs [20,22,50]. Structural analyses suggest that the molecular ruler responsible for determining cleavage positioning may lie in the spatial distance between the PAZ and RNase III domains, similarly to what has been observed in other DICER proteins [50]. Artificial mutations in key recognition residues within the PAZ domain (F1240A, Y1258A, and Y1263A) reduce the efficiency and accuracy of the second cleavage [22]. Additional analysis of the Coulomb potential map of DCL bound to pri-miRNA (PDB: 7ELD) [19] revealed that the PAZ domain aligns with a 15–17 nt internal loop while leaving additional spatial pockets corresponding to the 9–11 nt and 11–13 nt regions unoccupied [20].

The RNase III domains are essential for the precise excision of miRNA/miRNA* duplexes from pri-miRNA transcripts [19]. Both RNase III domains coordinate Mg^{2+} ions to hydrolyze the dsRNA, cleaving opposite RNA strands and generating characteristic 2 nt 3′ overhangs [56]. Similarly to the helicase domain, the RNase III domains are proposed to be autoinhibitory [57]. In the model derived by cryo-EM, RNase IIIa active site residues (Figure 3B) are in proximity to the miRNA and face the nucleic acid; however, inter-atomic distances are ~9 Å. Such distances

Box 1. Dissecting DCL1 activity through mutational landscapes

Researchers have identified several gain- and loss-of-function alleles of *DCL1* through mutant screening [28,52,57,86,87]. Hyperactive mutations, many of which were identified in *hyl1* suppressor screens [53,86,87], increase DCL1 processing efficiency and effectively bypass the presence of HYL1. The cryo-EM structures of DCL1 in complex with pri-miRNA and pre-miRNA, respectively (PDB: 7ELD and PDB: 7ELE [19]) help to speculate how hyperactive and hypoactive DCL1 mutant proteins might influence its structural and functional dynamics, and moreover allows the design of DCL1 mutant proteins that are impaired in specific cleavage functions. It is crucial to note here that this speculation is based on a medium-resolution atomic model that only reveals the general orientation of the protein secondary structure. Individual sidechains or flexible regions cannot be deduced from the cryo-EM map [19]. Despite these challenges, cryo-EM, augmented by predicted conformations, allows hypotheses to be made concerning functional aspects of DCL1 mutations (Figure I).

The E395K mutation in the hyperactive *dcl1-13* mutant introduces a positively charged lysine residue into the helicase domain [86]. This may increase structural stability by enabling interactions with N838 or the backbone of the DUF283 α-helix – a region that is implicated in HYL1 binding [55]. Similarly, the R363K mutation in *dcl1-20* may reduce steric hindrance at the interface between the helicase and DUF283, facilitating a more active conformation [53]. Three additional mutations – A355T, L377F, and V392M – appear to promote transitional helicase states. A355T, found in *dcl1-29*, may allow additional hydrogen bonding with Y389, whereas L377F in *dcl1-27* may enable π–π or S–aromatic interactions involving Y389, M393, or C380 of the DECH motif [87]. The V392M mutation in *dcl1-26* introduces higher conformational flexibility, although the interpretation is complicated by a second mutation in an unstructured region [87,88]. The R1495E mutation in *dcl1-23* is located near an unstructured region of the protein, making its structural consequences difficult to predict, even though it appears in the DCL1 structure model (PDB: 7ELD [19]).

By contrast, hypoactive mutants reveal how structural disruptions can impair enzymatic function. For example, the I431K mutation in *dcl1-8* likely rigidifies the helicase by electrostatic interactions with E435 or S414 of helicase the TAS motif III which is essential for ATP hydrolysis and RNA translocation [52,61,62]. The P415S mutation in *dcl1-7* may alter the catalytic role of TAS motif III and stiffen motif I through a new hydrogen bond with E270 [52]. Artificial mutations such as E1507Q and E1696Q, in *DCL1a** and *DCL1b** respectively, likely impair DCL1 catalytic activity by disrupting Mg^{2+} coordination in the RNase III domains [28,89]. Similarly, the G1692E mutation in *dcl1-15* introduces charge-induced steric clashes near an α-helix, possibly distorting the RNase IIIb domain [84].

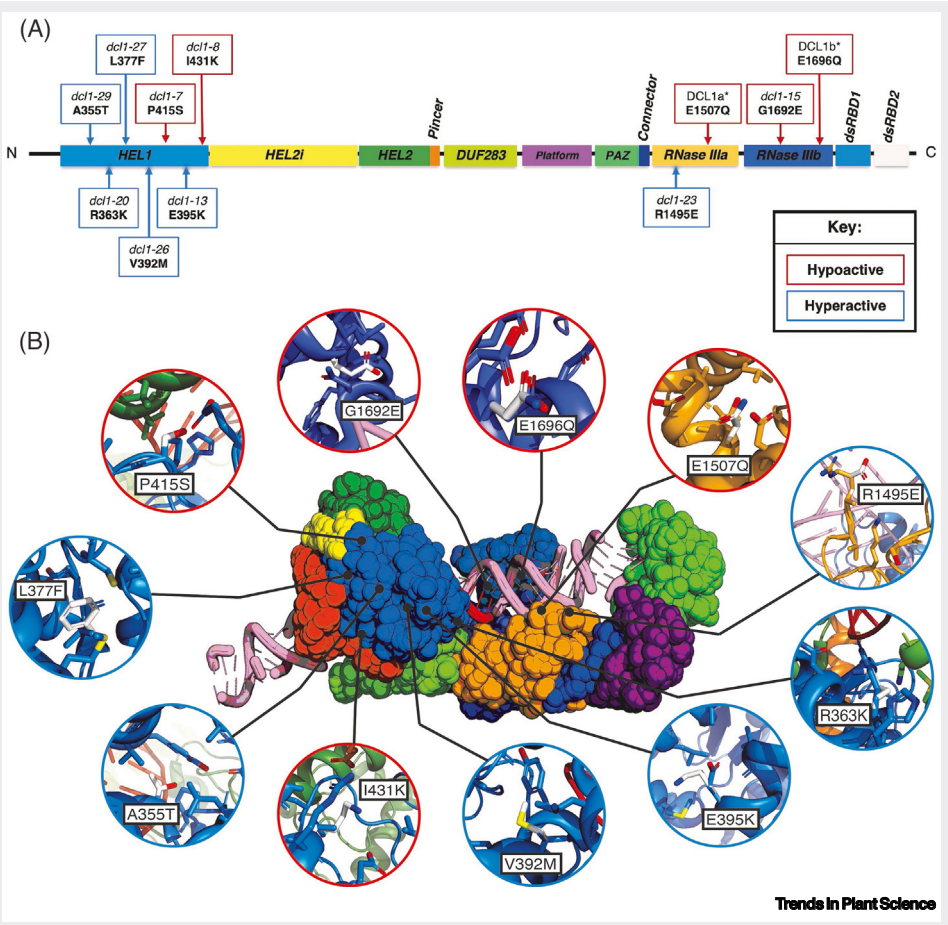

Figure I. Positions and structural environments of activity-altering mutations in DCL1. (A) Schematic illustration of DCL1 and the position of point mutations in the structured regions. (B) Detailed views highlight the positions and local structural environments of individual amino acid substitutions of hypo- and hyperactive DCL1 mutant proteins.

are relatively long for any mechanistic interpretation of an active complex state. Similar observations have been made for the RNase IIIb active site proximity (Figure 3B).

Although DCL1 has two dsRBD domains, only dsRBD1 significantly binds to dsRNA [58]. dsRBD2 acts as an adjuvant in RNA recognition and appears to be more important for protein–protein interaction and DCL1 localization [57,58]. The dsRBD1 domain interacting with the pri-miRNA is shown in Figure 3C, where it forms a complementary surface with the upstream part of the pri-miRNA. Molecular dynamics simulations suggest that specific residues such as R1736, Q1743, R1755, G1757, and N1758 may interact with RNA bases and potentially influence substrate recognition and positioning; in addition, they might induce conformational changes in the protein [59] (Figure 3C). There is a discrepancy between the binding mode observed in a high-quality reproduction of the human ADAR dsRBD1–RNA complex based on a nuclear magnetic resonance (NMR) structure (PDB: 2L2K) [60] and the cryo-EM map of DCL1, where the domain is only apparent at very low local resolution [19]. Both models show direct interactions of N1758 and R1736 (Figure 3C), whereas R1755 is present at the interface only in the NMR model [60]. R1736, which is strongly buried within the protein, exhibits a strong affinity for

A–C and U–C mismatches because these open the minor groove and may allow RNA differentiation by the dsRBD domain. At the same time, the presence of G would likely sterically hinder such interactions [59]. Despite these advances, much of the structure of DCL1 remains unresolved, particularly in unstructured regions that are crucial for interactions and regulation. Integrating advanced techniques such as cryo-EM, NMR, crosslinking mass spectrometry, and computational modeling will be essential to fully understand how specific residues influence DCL1 function [68].

DCL1 processing partners HYL1 and SE

Although DCL1 can process pri-miRNAs *in vitro* by itself [20,33], the presence of HYL1 and SE significantly increases cleavage efficiency and precision [11,20,61]. HYL1 consists of two N-terminal α1–β1–β2–β3–α2 folded dsRBDs [62] connected by a short unstructured linker of conserved length [63] and an unstructured C-terminal region [64]. Although both dsRBDs are essential for proper HYL1 functionality [65], the C-terminal unstructured region can be truncated without impairing the function of HYL1 [66]. The length of the linker restricts the positioning of the dsRBDs [67] but still allows flexibility in their conformation relative to each other [68]. Currently, NMR ensembles [69] and X-ray models [62] have resolved both the dsRBDs of HYL1, also in complex with RNA [62]. The full structure or domain proximity principles are unknown, but the available AlphaFold model (AF-O04492-F1) attributes a β-sandwich fold to the C-terminus with acceptable reliability. Interestingly, it is enriched in repeats which are predicted to be structurally similar to the pentapeptide repeats formed by A[N/D]LXX motifs [70].

Both dsRBD domains evolved early and have specialized functions [71]: dsRBD1 is believed to mediate direct binding to the miRNA/miRNA* duplex, and evidence from electrophoretic mobility shift assays indicates a preference for GC-rich sequences [34] (Figure 3D). To what extent this interaction is dependent on the 3D structure or on the primary sequence is unknown. Unlike canonical dsRBDs, the α2 region of HYL1 deviates from the well-conserved positively charged KKxAH motif, and is shortened and supported by a positively charged lysine of α1 for recognition of the major groove of the dsRNA backbone [72]. Surprisingly, canonical dsRBDs exhibit extensive interactions with the minor groove via their β2–β3 loop, whereas the same is dispensable for HYL1 binding to dsRNA *in vivo* [72].

The dsRBD of HYL1 exhibits weak dsRNA binding affinity [62] and is thought to be the main contributor to protein–protein interactions, including homodimerization [62,67,73] and interactions with DCL1 [55,57,71] and SE [64,67] (Figure 3D). Homodimerization is essential for its proper function in miRNA biogenesis: single point mutations that disrupt the putative dimerization interface cause reduced cleavage precision without affecting the interaction with DCL1 or SE [73]. Until now these conflicting findings have not been resolved and underline the need for 3D structure determination not only of DCL1, at higher resolution, but also of the miRNA processing complex.

SE is a protein of 720 amino acids that comprises an unstructured N-terminal sequence, a structured core domain, and a largely unstructured C-terminal region [64]. The N-terminal region in SE is essential for the formation of Dicing bodies (D-bodies) through liquid–liquid phase separation [74]. Earlier studies suggest that the N-terminal region is responsible for the RNA-binding function of SE, but later studies found that SE lacking the N-terminal region could still bind to pri-miRNAs [61,74]. The C-terminal part of SE is dispensable for SE binding to DCL1 and or RNA *in vitro*, but might play important roles in SE protein turnover (Figure 3D) [41,42,61,75]. Currently, only the core domain has been resolved at 2.74 Å by X-ray crystallography [64]. The SE core consists of two N-terminal α-helices, an α–α–α–β–β–α–α–α folded mid-domain interspersed with

unstructured loops, and a C-terminal β–β–β–α folded C_2H_2 zinc-finger motif encased by two α-helices [64]. The zinc finger is crucial for the interaction with DCL1 *in vitro* [61], and mutations of the zinc-binding amino acids lead to a complete loss of function *in vivo* [64]. The SE core interacts with the helicase and PAZ of DCL1 and the dsRBD2 of HYL1 [64] (Figure 3D), whereas the two α-helices of the SE core and the SE mid-domain interact with HYL1 dsRBD2 (Figure 3D) [64].

Although degradome sequencing revealed that the majority of the first cutting events of pri-miRNAs rely on HYL1 and SE, it is surprising that a substantial fraction of pri-miRNAs are processed in a HYL1- and/or SE-independent manner [20]. In line with these observations, cold temperatures appear to reduce the dependence on SE and HYL1 for miRNA production [76]. GC base pairs (and therefore high energy) in the pri-miRNA make HYL1 less important at cold temperatures [76]. This highlights that, to uncover the precise functions of SE and HYL1 in DCL1-mediated processing, a combination of *in silico, in vitro,* and *in planta* data will be essential. This integrated approach is crucial for unraveling how these factors operate under diverse conditions and in response to different biological stimuli. In addition, the 3D structure of the DCL1–SE–HYL1 complex not only could explain or verify the target specificity of the miRNA processing complex but could also illuminate the intricate modulation of DCL1 processing efficiency and accuracy via its accessory proteins.

Concluding remarks and future perspectives

The interaction between diverse pri-miRNA structures and the plant miRNA processing complex underscores the complexity of miRNA biogenesis. Extensive research has identified key structural elements of pri-miRNAs such as internal loops, sequence motifs, and mismatch positions [20,21,32,33]. With the growing availability of *in vivo* RSSs of pri-miRNAs and structural information on DCL1, the *cis* and *trans* determinants that guide pri-miRNA cleavage are becoming increasingly clear [19,41–44,76,77]. Future research should focus on understanding the dynamic nature of RSS, which can be influenced by environmental conditions, RNA modifications, and interactions with other proteins. Studies in humans suggest that the RSS of the nascent transcriptome is highly plastic and strongly influenced by RNA polymerase II elongation speed [78]. Given the importance of RSS for precise plant pri-miRNA processing, factors that influence transcription dynamics may significantly affect miRNA biogenesis and should therefore be thoroughly investigated in future studies. In plants, Gonzalo *et al.* showed that LTB processing occurs fully cotranscriptionally, whereas in BTL processing only the first cleavage takes place cotranscriptionally, and the second cleavage occurs post-transcriptionally [79]. It remains unclear whether structural rearrangements occur during the transition of pre-miRNAs from chromatin to the nucleoplasm. In addition, proteins such as PRP40, which control the cotranscriptional assembly and dynamics of the miRNA processing complex, may influence RSS directly or indirectly [80]. Apart from the dynamic RSS within individual plants, there is also significant intraspecific and interspecific variation not only in pri-miRNAs (Box 2) but also in miRNA biogenesis factors [81]. How this intra- and interspecific

Box 2. Diversity of pri-miRNAs in the plant kingdom

Polymorphisms in pri-miRNA structures can lead to differences in miRNA abundance and functionality across different plant species [90–93]. Single-nucleotide polymorphisms (SNPs), insertions, or deletions observed in geographically distinct arabidopsis accessions alter pri-miRNA secondary structures, including disruption of conserved structural motifs such as the 15–17 nt ruler. These structural changes can significantly impair DCL1 recognition and consequently reduce miRNA accumulation [90,91]. In arabidopsis, intraspecific variation such as SNPs within pri-miRNAs impacts on their processing efficiency, thereby influencing phenotypic traits such as leaf morphology [77]. A particularly interesting example of miRNA gene variation across plant species is *MIR858*. Exclusive to seed plants, *MIR858* harbors an extended hairpin structure ranging from 250 nt to 3500 nt [94]. This unique, non-canonical structure originated from the inverted duplication of two ancestral TT2-like *MYB* genes, resulting in high pri-miR858 hairpin length variation among seed plants [94]. The presence of variable loop lengths suggests that structural divergence in miRNAs has led to species-specific regulatory mechanisms [94].

Outstanding questions

What is the complete 3D structural arrangement and dynamics of the DCL1–SE–HYL1 complex, and how does this structure influence processing efficiency, accuracy, and flexibility?

What are the exact structure-based interactions involved in DCL1 organization and in pri-miRNA binding, recognition, and processing?

How do additional protein interactors of the DCL1–SE–HYL1 complex mechanistically influence its activity, specificity, or structural conformation, and do these interactions actively remodel the RSSs of pri-miRNAs?

Why is the processing of some pri-miRNAs dependent on HYL1 and SE whereas that of other pri-miRNAs is not?

How do recent structural and biochemical insights into the DCL1–SE–HYL1 complex and the RSS of pri-miRNAs correlate with cellular-level mechanisms of pri-miRNA processing, including the dynamics of co- versus post-transcriptional cleavage events or the formation and function of D-bodies?

How does natural intra- and interspecific variation in both pri-miRNA structures and the miRNA-processing machinery (such as DCL1 and its accessory proteins) contribute to differences in miRNA processing efficiency, accuracy, and isomiR generation, and could these variations provide adaptive advantages under some conditions?

variation contributes to changes in processing modes, processing efficiency, or the generation of isomiRs is largely unexplored and awaits investigation (see Outstanding questions).

Challenges remain in accurately modeling the interactions between DCL1 and structurally diverse pri-miRNAs, and this reflects the broader difficulty of reliably predicting protein–RNA interactions [82]. Future research should integrate biochemical approaches, structural biology techniques, and computational modeling to elucidate the complete 3D architecture of the miRNA processing complex across diverse plant species and pri-miRNA substrates. Resolving the structural determinants that underlie miRNA specificity and precise processing will enhance our understanding of gene regulation and may facilitate novel genome-editing strategies in both fundamental research and agricultural applications because even single-nucleotide modifications can substantially impact on pri-miRNA processing and consequently affect plant traits [83].

Acknowledgments

This work was supported by the Deutsche Forschungsgemeinschaft (DFG-514901783) through the Collaborative Research Centre 1664 'Plant Proteoform Diversity–SNP2Prot' (projects A05 and C04).

Declaration of interests

The authors declare no competing interests.

Declaration of generative artificial intelligence and artificial intelligence-assisted technologies in the writing process

During the preparation of this work the authors used ChatGTP for language editing, including spelling correction and readability improvements. No intellectual contribution, conceptualization, or original content generation was performed by language models. After using this tool, the authors reviewed and edited the content as needed and take full responsibility for the content of the publication.

References

1. Zhan, J. and Meyers, B.C. (2023) Plant small RNAs: their biogenesis, regulatory roles, and functions. *Annu. Rev. Plant Biol.* 74, 21–51
2. Mencia, R. *et al.* (2023) Keeping up with the miRNAs: current paradigms of the biogenesis pathway. *J. Exp. Bot.* 74, 2213–2227
3. Zhao, X. *et al.* (2025) MicroRNAs in plant development and stress resistance. *Plant Cell Environ.* 48, 5909–5929
4. Bajczyk, M. *et al.* (2023) Recent insights into plant miRNA biogenesis: multiple layers of miRNA level regulation. *Plants* 12, 342
5. Jodder, J. (2021) Regulation of pri-MIRNA processing: mechanistic insights into the miRNA homeostasis in plant. *Plant Cell Rep.* 40, 783–798
6. Cambiagno, D.A. *et al.* (2021) HASTY modulates miRNA biogenesis by linking pri-miRNA transcription and processing. *Mol. Plant* 14, 426–439
7. Bologna, N.G. *et al.* (2018) Nucleo-cytosolic shuttling of ARGONAUTE1 prompts a revised model of the plant microRNA pathway. *Mol. Cell* 69, 709–719
8. Dalmadi, Á. *et al.* (2021) Controlled RISC loading efficiency of miR168 defined by miRNA duplex structure adjusts ARGONAUTE1 homeostasis. *Nucleic Acids Res.* 49, 12912–12928
9. Jungers, C.F. and Djuranovic, S. (2022) Modulation of miRISC-mediated gene silencing in eukaryotes. *Front. Mol. Biosci.* 9, 832916
10. Fang, Y. and Spector, D.L. (2007) Identification of nuclear dicing bodies containing proteins for microRNA biogenesis in living *Arabidopsis* plants. *Curr. Biol.* 17, 818–823
11. Dong, Z. *et al.* (2008) The RNA-binding proteins HYL1 and SE promote accurate in vitro processing of pri-miRNA by DCL1. *Proc. Natl. Acad. Sci. U. S. A.* 105, 9970–9975
12. Tan, H. *et al.* (2020) The diversity of post-transcriptional gene silencing mediated by small silencing RNAs in plants. *Essays Biochem.* 64, 919–930
13. Zhang, S. *et al.* (2015) New insights into pri-miRNA processing and accumulation in plants. *Wiley Interdiscip. Rev. RNA* 6, 533–545
14. Modepalli, V. *et al.* (2018) The methyltransferase HEN1 is required in Nematostella vectensis for microRNA and piRNA stability as well as larval metamorphosis. *PLoS Genet.* 14, e1007590
15. Li, J. *et al.* (2005) Methylation protects miRNAs and siRNAs from a 3′-end uridylation activity in *Arabidopsis*. *Curr. Biol.* 15, 1501–1507
16. Kim, H. *et al.* (2024) The biogenesis and regulation of animal microRNAs. *Nat. Rev. Mol. Cell Biol.* 26, 276–296
17. Axtell, M.J. *et al.* (2011) Vive la différence: biogenesis and evolution of microRNAs in plants and animals. *Genome Biol.* 12, 221
18. Moran, Y. *et al.* (2017) The evolutionary origin of plant and animal microRNAs. *Nat. Ecol. Evol.* 1, 0027
19. Wei, X. *et al.* (2021) Structural basis of microRNA processing by Dicer-like 1. *Nat Plants* 7, 1389–1396
20. Yan, X. *et al.* (2024) Parallel degradome-seq and DMS-MaPseq substantially revise the miRNA biogenesis atlas in *Arabidopsis*. *Nat Plants* 10, 1126–1143
21. Rosatti, S. *et al.* (2024) Principles of miRNA/miRNA* function in plant MIRNA processing. *Nucleic Acids Res.* 52, 8356–8369
22. Zhang, H. and Li, F. (2024) Structural determinants in the miRNA/miRNA* duplex and the DCL1 PAZ domain for precise and efficient plant miRNA processing. *Plant J.* 120, 109–122
23. Cuperus, J.T. *et al.* (2011) Evolution and functional diversification of MIRNA genes. *Plant Cell* 23, 431–442
24. Song, L. *et al.* (2010) RNA secondary structural determinants of miRNA precursor processing in *Arabidopsis*. *Curr. Biol.* 20, 37–41
25. Mateos, J.L. *et al.* (2010) Identification of microRNA processing determinants by random mutagenesis of *Arabidopsis* MIR172a precursor. *Curr. Biol.* 20, 49–54
26. Werner, S. *et al.* (2010) Structure determinants for accurate processing of miR172a in *Arabidopsis thaliana*. *Curr. Biol.* 20, 42–48
27. Bologna, N.G. *et al.* (2013) Multiple RNA recognition patterns during microRNA biogenesis in plants. *Genome Res.* 23, 1675–1689

28. Zhu, H. *et al.* (2013) Bidirectional processing of pri-miRNAs with branched terminal loops by *Arabidopsis* Dicer-like 1. *Nat. Struct. Mol. Biol.* 20, 1106–1115
29. Vivek, A.T. *et al.* (2024) AthisomiRDB: a comprehensive database of *Arabidopsis* isomiRs. *Database* 2024, baae115
30. Zhu, R. *et al.* (2016) Discovering numerical differences between animal and plant microRNAs. *PLoS One* 11, e0165152
31. Chorostecki, U. *et al.* (2017) Evolutionary footprints reveal insights into plant microRNA biogenesis. *Plant Cell* 29, 1248–1261
32. Rojas, A.M.L. *et al.* (2020) Identification of key sequence features required for microRNA biogenesis in plants. *Nat. Commun.* 11, 5320
33. Hirata, R. *et al.* (2022) Unpaired nucleotides on the stem of microRNA precursor are important for precise cleavage by Dicer-like 1 in *Arabidopsis*. *Genes Cells* 27, 280–292
34. Narjala, A. *et al.* (2020) A conserved sequence signature is essential for robust plant miRNA biogenesis. *Nucleic Acids Res.* 48, 3103–3118
35. Ho, T. *et al.* (2007) Evidence for targeting common siRNA hotspots and GC preference by plant Dicer-like proteins. *FEBS Lett.* 581, 3267–3272
36. Ho, T. *et al.* (2008) Evidence for GC preference by monocot Dicer-like proteins. *Biochem. Biophys. Res. Commun.* 368, 433–437
37. Yan, F. *et al.* (2010) Characterization of siRNAs derived from rice stripe virus in infected rice plants by deep sequencing. *Arch. Virol.* 155, 935–940
38. Iki, T. *et al.* (2018) Structural elexibility enables alternative maturation, ARGONAUTE sorting and activities of miR168, a global gene silencing regulator in plants. *Mol. Plant* 11, 1008–1023
39. Vandivier, L.E. *et al.* (2016) The conservation and Ffunction of RNA secondary structure in plants. *Annu. Rev. Plant Biol.* 67, 463–488
40. Yang, X. *et al.* (2018) New era of studying RNA secondary structure and its influence on gene regulation in plants. *Front. Plant Sci.* 9, 671
41. Zhong, S. *et al.* (2024) SERRATE drives phase separation behaviours to regulate m6A modification and miRNA biogenesis. *Nat. Cell Biol.* 26, 2129–2143
42. Wang, Z. *et al.* (2018) SWI2/SNF2 ATPase CHR2 remodels pri-miRNAs via Serrate to impede miRNA production. *Nature* 557, 516–521
43. Li, X. *et al.* (2024) RNA helicase Brr2a promotes miRNA biogenesis by properly remodelling secondary structure of pri-miRNAs. *Nat Plants* 10, 1532–1547
44. Bhat, S.S. *et al.* (2020) mRNA adenosine methylase (MTA) deposits m^6A on pri-miRNAs to modulate miRNA biogenesis in *Arabidopsis thaliana*. *Proc. Natl. Acad. Sci.* 117, 21785–21795
45. Mondol, V. *et al.* (2015) Splicing remodels the let-7 primary microRNA to facilitate Drosha processing in Caenorhabditis elegans. *RNA* 21, 1396–1403
46. Contrant, M. *et al.* (2014) Importance of the RNA secondary structure for the relative accumulation of clustered viral microRNAs. *Nucleic Acids Res.* 42, 7981–7996
47. Fukudome, A. and Fukuhara, T. (2017) Plant dicer-like proteins: double-stranded RNA-cleaving enzymes for small RNA biogenesis. *J. Plant Res.* 130, 33–44
48. Liu, Q. *et al.* (2009) Dicer-like (DCL) proteins in plants. *Funct. Integr. Genomics* 9, 277–286
49. Roy, P. and Datta, A. (2017) DCL and associated proteins of *Arabidopsis thaliana* – an interaction study. *Int. Lett. Nat. Sci.* 61, 85–94
50. Zapletal, D. *et al.* (2023) Dicer structure and function: conserved and evolving features. *EMBO Rep.* 24, e57215
51. Su, L.-Y. *et al.* (2024) The origin, evolution, and functional divergence of the Dicer-like (DCL) and Argonaute (AGO) gene families in plants. *Epigenet. Insights* 17, e003
52. Schauer, S.E. *et al.* (2002) DICER-LIKE1: blind men and elephants in *Arabidopsis* development. *Trends Plant Sci.* 7, 487–491
53. Liu, C. *et al.* (2012) The helicase and RNaseIIIa domains of *Arabidopsis* Dicer-like1 modulate catalytic parameters during microRNA miogenesis. *Plant Physiol.* 159, 748–758
54. Byrd, A., .K. (2012) Superfamily 2 helicases. *Front. Biosci.* 17, 2070
55. Qin, H. *et al.* (2010) Structure of the *Arabidopsis thaliana* DCL4 DUF283 domain reveals a noncanonical double-stranded RNA-binding fold for protein–protein interaction. *RNA* 16, 474–481
56. Ciechanowska, K. *et al.* (2021) Genetic insight into the domain structure and functions of Dicer-type ribonucleases. *Int. J. Mol. Sci.* 22, 616
57. Liu, Q. *et al.* (2013) Complementation of Hyponastic Leaves1 by double-strand RNA-binding domains of Dicer-like1 in nuclear dicing bodies. *Plant Physiol.* 163, 108–117
58. Suarez, I.P. *et al.* (2015) Induced folding in RNA recognition by *Arabidopsis thaliana* DCL1. *Nucleic Acids Res.* 43, 6607–6619
59. Drusin, S.I. *et al.* (2016) dsRNA–protein interactions studied by molecular dynamics techniques. Unravelling dsRNA recognition by DCL1. *Arch. Biochem. Biophys.* 596, 118–125
60. Stefl, R. *et al.* (2010) The solution structure of the ADAR2 dsRBM–RNA complex reveals a sequence-specific readout of the minor groove. *Cell* 143, 225–237
61. Iwata, Y. *et al.* (2013) Dissecting the interactions of SERRATE with RNA and DICER-LIKE 1 in *Arabidopsis* microRNA precursor processing. *Nucleic Acids Res.* 41, 9129–9140
62. Yang, S.W. *et al.* (2010) Structure of *Arabidopsis* HYPONASTIC LEAVES1 and its molecular implications for miRNA processing. *Struct. Lond. Engl. 1993* 18, 594–605
63. Mascali, F.C. *et al.* (2023) Conserved linker length in double dsRBD proteins from plants restricts interdomain motion. *J. Magn. Reson. Open* 16–17, 100109
64. Machida, S. *et al.* (2011) Molecular insights into miRNA processing by *Arabidopsis thaliana* SERRATE. *Nucleic Acids Res.* 39, 7828–7836
65. Reis, R.S. *et al.* (2016) Chimeric DCL1-partnering proteins provide insights into the microRNA pathway. *Front. Plant Sci.* 6, 1201
66. Wu, F. *et al.* (2007) The N-terminal double-stranded RNA binding domains of *Arabidopsis* HYPONASTIC LEAVES1 are sufficient for pre-microRNA processing. *Plant Cell* 19, 914–925
67. Achkar, N.P. *et al.* (2018) A quick HYL1-dependent reactivation of microRNA production is required for a proper developmental response after extended periods of light deprivation. *Dev. Cell* 46, 236–247
68. Wieczorek, P. *et al.* (2023) Solution structure and behaviour of the *Arabidopsis thaliana* HYL1 protein. *Biochim. Biophys. Acta BBA Gen. Subj.* 1867, 130376
69. Rasia, R.M. *et al.* (2010) Structure and RNA interactions of the plant microRNA processing-associated protein HYL1. *Biochemistry* 49, 8237–8239
70. Buchko, G.W. *et al.* (2008) Insights into the structural variation between pentapeptide repeat proteins – crystal structure of Rfr23 from *Cyanothece* 51142. *J. Struct. Biol.* 162, 184–192
71. Jia, H. *et al.* (2021) Direct molecular evidence for an ancient, conserved developmental toolkit controlling posttranscriptional gene regulation in land plants. *Mol. Biol. Evol.* 38, 4765–4777
72. Burdisso, P. *et al.* (2014) Structural determinants of *Arabidopsis thaliana* hyponastic leaves 1 function in vivo. *PLoS One* 9, e113243
73. Yang, X. *et al.* (2014) Homodimerization of HYL1 ensures the correct selection of cleavage sites in primary miRNA. *Nucleic Acids Res.* 42, 12224–12236
74. Xie, D. *et al.* (2021) Phase separation of SERRATE drives dicing body assembly and promotes miRNA processing in *Arabidopsis*. *Nat. Cell Biol.* 23, 32–39
75. Li, Y. *et al.* (2020) Degradation of SERRATE via ubiquitin-independent 20S proteasome to survey RNA metabolism. *Nat Plants* 6, 970–982
76. Ré, D.A. *et al.* (2019) Alternative use of miRNA-biogenesis co-factors in plants at low temperatures. *Development* 146, dev172932
77. Todesco, M. *et al.* (2012) Natural variation in biogenesis efficiency of individual *Arabidopsis thaliana* microRNAs. *Curr. Biol.* 22, 166–170
78. Saldi, T. *et al.* (2021) Alternative RNA structures formed during transcription depend on elongation rate and modify RNA processing. *Mol. Cell* 81, 1789–1801
79. Gonzalo, L. *et al.* (2022) R-loops at microRNA encoding loci promote co-transcriptional processing of pri-miRNAs in plants. *Nat Plants* 8, 402–418

80. Stepien, A. *et al.* (2022) Chromatin-associated microprocessor assembly is regulated by the U1 snRNP auxiliary protein PRP40. *Plant Cell* 34, 4920–4935
81. 1001 Genomes Consortium (2016) 1,135 Genomes reveal the global pattern of polymorphism in *Arabidopsis thaliana*. *Cell* 166, 481–491
82. Zeng, C. *et al.* (2024) Advances and challenges in scoring functions for RNA–protein complex structure prediction. *Biomolecules* 14, 1245
83. Deng, F. *et al.* (2022) Molecular evolution and functional modification of plant miRNAs with CRISPR. *Trends Plant Sci.* 27, 890–907
84. Willmann, M.R. *et al.* (2011) MicroRNAs regulate the timing of embryo maturation in *Arabidopsis*. *Plant Physiol.* 155, 1871–1884
85. Foley, S.W. *et al.* (2017) A global view of RNA–protein interactions identifies post-transcriptional regulators of root hair cell fate. *Dev. Cell* 41, 204–220
86. Tagami, Y. *et al.* (2009) A dominant mutation in DCL1 suppresses the hyl1 mutant phenotype by promoting the processing of miRNA. *RNA* 15, 450–458
87. Gao, S. *et al.* (2020) Hyponastic leaves 1 protects pri-miRNAs from nuclear exosome attack. *Proc. Natl. Acad. Sci. U. S. A.* 117, 17429–17437
88. Aledo, J.C. (2019) Methionine in proteins: the Cinderella of the proteinogenic amino acids. *Protein Sci.* 28, 1785–1796
89. Drusin, S.I. *et al.* (2020) Study of the role of Mg^{2+} in dsRNA processing mechanism by bacterial RNase III through QM/MM simulations. *J. Biol. Inorg. Chem.* 25, 89–98
90. Jaganathan, D. *et al.* (2023) A conserved SNP variation in the pre-miR396c flanking region in *Oryza sativa* indica landraces correlates with mature miRNA abundance. *Sci. Rep.* 13, 2195
91. Tripathi, A.M. *et al.* (2023) Indian Himalayan natural *Arabidopsis thaliana* accessions with abolished miR158 levels exhibit robust miR173-initiated trans-acting cascade silencing. *Plant J.* 114, 855–874
92. Ehrenreich, I.M. and Purugganan, M.D. (2008) Sequence variation of microRNAs and their binding sites in *Arabidopsis*. *Plant Physiol.* 146, 1974–1982
93. Chen, J. *et al.* (2016) Genetic variations and miRNA–target interactions contribute to natural phenotypic variations in *Populus*. *New Phytol.* 212, 150–160
94. Wang, W. *et al.* (2024) Identification of miRNA858 long-loop precursors in seed plants. *Plant Cell* 36, 1637–1654